East European Journal of Physics. **1.** 278-287 (2024)
DOI:10.26565/2312-4334-2024-1-24 ISSN 2312-4334

# $La_{0.8}Bi_{0.2}FeO_3$ PEROVSKITE-TYPE: HIGH-PERFORMANCE OF PHOTOCATALYTIC DEGRADATION OF ORTHO-TOLUIDINE BLUE UNDER VISIBLE LIGHT IRRADIATION

**Ouarda Ben Ali[a], Mohammed Sadok Mahboub[a]*, Soria Zeroual[a], Samir Bayou[b], Azzeddine Beggas[a], Mebrouk Ghougali[a], Adel Benarfa[c], Souhaila Meneceur[d]**
[a] *LEVRES Laboratory, University of El Oued, 39000 El Oued, Algeria*
[b] *Chemistry department, Faculty of Exact Sciences, University of El Oued, 39000 El Oued, Algeria*
[c] *Centre de Recherche Scientifique et Technique en Analyses Physico-Chimiques (CRAPC)-PTAPC, P.O. Box 0354, Laghouat 03000, Algeria*
[d] *Laboratory of Biotechnology biomaterial and condensed matter, Faculty of Technology, University of El Oued, El-Oued 39000, Algeria*
**Corresponding author e-mail: mahboub-mohammedsadok@univ-eloued.dz*
Received January 5, 2024; revised February 5, 2024; accepted February 17, 2024

In this study, $La_{1-x}Bi_xFeO_3$ (x=0.0, 0.2, 0.4, and 0.6) perovskite nanoparticles were synthesized by a modified Pechini method. Rigorous analysis through XRD and SEM/EDX confirmed the absence of secondary phases in both pure and Bi-substituted $LaFeO_3$ samples, indicating the formation of a single-phase perovskite. SEM images revealed the quasi-spherical shape of the particles. The photocatalytic activity of $La_{1-x}Bi_xFeO_3$ (x=0.0, 0.2, 0.4, and 0.6) was evaluated by the degradation of ortho-Toluidine Blue under visible light irradiation, indicating that $La_{0.8}Bi_{0.2}FeO_3$ exhibited excellent photocatalytic activity. The overall removal rate of o-Toluidine Blue reached 90.09% after visible light irradiation lasting for 60 min. We attribute this heightened photocatalytic activity to the grain size and optical properties of prepared sample. Consequently, the $La_{0.8}Bi_{0.2}FeO_3$ can be considered as a very promising photocatalyst in future industrial application to treat effectively wastewater of dyes.
**Keywords:** *$La_{1-x}Bi_xFeO_3$; Ortho-Toluidine Blue dye; Modified Pechini method; Visible-light photocatalysis; Wastewater treatment*
**PACS:** 81.20.Ka, 81.16.Hc, 89.60.-k

## INTRODUCTION

The rapid expansion of urbanization and industrialization, coupled with soaring global population growth, has significantly exacerbated the issue of water pollution [1]. Approximately 1.2 billion people worldwide, particularly in developing nations, grapple with the alarming consequences of water contamination, which extend far beyond environmental degradation [2]. Water pollutants pose a grave threat to human health, contributing to respiratory disorders, dermatitis, asthma, mutagenicity, and even cancer and other diseases [2-7]. This dire scenario underscores the need for innovative and effective wastewater treatment technologies. Dye wastewater is one of the most difficult degradable industrial wastewater, due to its variety, complicated organic composition and poor biochemical degradability, even including toxic ingredients which can weaken the microbial mineralization of organic pollutants and lead to the destruction of water ecological system[8]. Effective wastewater treatment plays a pivotal role in safeguarding public health and the environment. This vital process involves the removal of contaminants and pollutants from wastewater, rendering it suitable for safe discharge into the ecosystem or potential reuse. However, the complexity and scale of this challenge have prompted the exploration of innovative, sustainable solutions [9].

In recent years, photocatalytic technologies have emerged as promising strategies for advanced wastewater treatment [10-12]. These methods harnesses the power of photocatalysts, typically semiconducting materials, to accelerate the degradation of both organic and inorganic pollutants when exposed to light irradiation. Semiconductor photocatalysis, in particular, has attracted considerable attention due to its cost-effectiveness, non-toxicity, high chemical and thermal stability, and eco-friendly nature [13,14]. Traditional semiconductor photocatalysts, like $TiO_2$ [15, 16], ZnO [15, 17], and $SnO_2$[18], have been extensively employed in photocatalysis due to their affordability, stability, and low environmental impact. However, their limited ability to utilize solar energy, primarily in the UV range, has driven the exploration of narrow band gap semiconductors, which can absorb a broader spectrum of solar radiation, especially in the visible light region [19].

Perovskite materials, have emerged as a compelling class of narrow band gap semiconductors for photocatalytic applications [20]. Their unique structural characteristics and synthesis processes significantly influence their photocatalytic efficiency, making them versatile for diverse applications, including gas sensing [21], water splitting [22], and the photocatalytic degradation of organic pollutants [23, 24]. Among the narrow band gap semiconductors, $LaFeO_3$ stands out as a promising photocatalyst, with several studies emphasizing its synthesis and efficacy in the photodegradation of organic dyes under visible light irradiation [25-28]. $LaFeO_3$, with a narrow band gap of only 2.0 eV, exhibits exceptional potential for utilizing visible light from the solar spectrum, rendering it highly suitable for

***Cite as***: O. Ben Ali, M.S. Mahboub, S. Zeroual, S. Bayou, A. Beggas, M. Ghougali, A. Benarfa, S. Meneceur, East Eur. J. Phys. 1, 278 (2024), https://doi.org/10.26565/2312-4334-2024-1-24

photocatalysis under sunlight [29]. Its outstanding photocatalytic properties have propelled $LaFeO_3$ into the spotlight, attracting attention for its applications in water treatment.

The catalytic performance of $LaFeO_3$ perovskite in wastewater dye removal processes has been investigated. Thirumalairajan et al. [30] studied the catalytic activity of the $LaFeO_3$ microsphere to degrade Rhodamine B (RhB), whereas Deng et al. [31] studied its adsorption behaviour for RhB. On another hand, Mocwana et al. [32] studied the activity of the lanthanum ferrite using the photocatalytic degradation of ortho-toluidine blue (o-TB) under visible light. To further enhance the photocatalytic performance of $LaFeO_3$, modification strategies, such as doping with various elements, have been widely explored [33]. In this context, Cu-doped $LaFeO_3$ catalysts have demonstrated remarkable efficiency in the decolorization of both cationic and anionic dyes under visible light irradiation [34]. Also, experiments of radical trapping in Sr-doped porous $LaFeO_3$ samples reveal that •OH species are dominant intermediate oxidants involved in the oxidation of 2,4-DCP and RhB over the optimized sample [35].

The visible light-driven degradation of o-Toluidine Blue (o-TB) will be the focus of this investigation, shedding light on the potential of Bi-substituted $LaFeO_3$ perovskite photocatalysis in addressing these pressing challenges. Photocatalysis can be used to degrade or break down certain organic compounds, including dyes like o-TB, that may be present in water and contribute to water pollution. The effect of photocatalysis on o-TB as a water dye may result in the degradation of the dye molecules, reducing its concentration in the water. This process can be effective in treating water contaminated with certain organic dyes, which are common pollutants in industrial wastewater. In this study, the structural, morphological, optical evaluation and photocatalytic performance of a series of $La_{1-x}Bi_xFeO_3$ ($x$=0.0, 0.2, 0.4, and 0.6) would be emphatically discussed.

## EXPERIMENTAL

### Material Preparation

The technique of modified Pechini method was employed for the synthesis of Bismuth-doped Lanthanum ferrite $La_{1-x}Bi_xFeO_3$. Specifically, precise amounts of Lanthanum nitrate ($La(NO_3)_3{\cdot}6H_2O$, Sigma-Aldrich, ≥99.0%), Bismuth nitrate ($Bi(NO_3)_3{\cdot}5H_2O$, Sigma-Aldrich, ≥98.0%), and Ferric nitrate ($Fe(NO_3)_3{\cdot}9H_2O$, Sigma-Aldrich, ≥98.0%)were utilized as initial reagents to produce $La_{1-x}Bi_xFeO_3$(x = 0, 0.2, 0.4, and 0.6). The raw materials were dissolved in 100 ml of double-distilled water to create a transparent solution, which was then evaporated at 60 °C while being continuously stirred using a magnetic stirrer. Additionally, nitric acid was incrementally introduced during the stirring process to regulate the pH. The solution was then supplemented with citric acid (Sigma-Aldrich, ≥98.0%), Ethylene Diamine Tetra Acetic acid (EDTA, Sigma-Aldrich, ≥98.0%), and ethylene glycol (Sigma-Aldrich, ≥98.0%), as well as other chemicals to create a brown precursor solution. The solution is then heated to 120 °C (10 °C/min) until it solidifies into a dry gel. The gel then turns into a puff as the temperature rises to 350 °C. The resulting puff was dried for 10 hours at 110 °C to produce a dark brown powder, and the soft powders were then calcined for 12 hours at 600 °C with a 5 °C/min rate. The light brown powder was then heated for 24 hours at 800 °C in the air using a tubular furnace (R 50/500/13 Nabertherm model). To obtain the phase, this operation is repeated twice (Fig. 1).

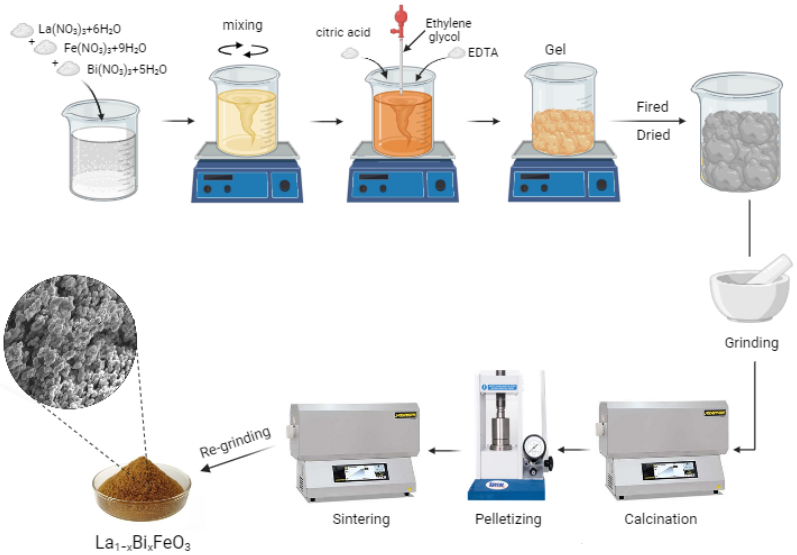


**Figure 1.** Schematic representation of the elementary steps of $La_{1-x}Bi_xFeO_3$ ($x$ = 0.0,0.2, 0.4, 0.6) perovskite preparation using the modified Pechini method

### Material Characterization

Phase identification and unit cell parameter determination were checked using powder X-ray diffraction (XRD) at room temperature. Powder X-ray diffraction (PXRD) patterns were recorded on a Proto AXRD Benchtop diffractometer in Bragg-Brentano θ-2θ-geometry with $CuK_\alpha$ radiation (λ=1.5418 Å) operating at 30 kV and 20 mA. Regarding the

examination of the synthesized samples, their morphology was investigated utilizing a Thermo Scientific Quattro ESEM scanning electron microscope. Simultaneously, the compositions were analyzed using energy dispersive X-ray (EDX) spectroscopy, employing a Zeiss SmartEDX detector integrated into the Zeiss Evo15 Scanning Electron Microscope (SEM). This setup is designed for observing dry and conducting samples. In addition, Fourier transform infrared (FTIR) spectra were recorded in the range of 2000-450 $cm^{-1}$ using an IR Spirit - Shimadzu Fourier transform infrared (FTIR) spectrometer. The as-synthesized powders were also analyzed using a Shimadzu UV-visible spectrometer, specifically the Shimadzu UV-1900.

### Photocatalytic Activity

In this study, we investigate the photocatalytic degradation of o-TB in the presence of $La_{1-x}Bi_xFeO_3$ ($x$ = 0.0, 0.2, 0.4, 0.6). The experimental work begins by adding 5 mg of the catalyst to a 5 ml o-TB solution. The prepared solution is made using distilled water at a concentration of $4x10^{-5}$mol/L. Following this, the solution is exposed to sunlight for varying durations (10, 20, 30, and 60 min) at room temperature and a neutral pH. On the other hand, the catalyst is separated through centrifugation, and a spectrophotometer (Shimadzu 1900 model) is used to detect absorbance values at 629 nm. Furthermore, the calculation method for degradation efficiency is presented in the following equation:

$$\text{degradation}(\%) = \frac{(C_0 - C_t)}{C_0} \times 100. \quad (1)$$

Where $C_0$is the concentration of o-TB solution at the reaction's beginning and $C_t$ its concentration of pollutants at time t.

## RESULTS AND DISCUSSION

### Structural, Morphological and Elemental Analysis

In Fig. 2, the X-Ray Powder Diffraction patterns of the pure and $Bi^{3+}$-substituted $LaFeO_3$samples are displayed.

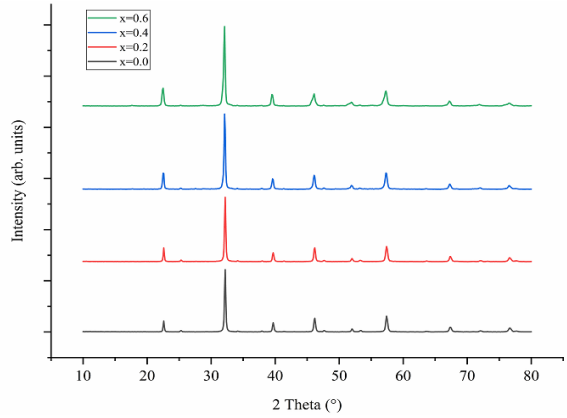


**Figure 2.** X-Ray powder diffraction pattern of $La_{1-x}Bi_xFeO_3$ (a) x=0.0, (b) x=0.2 (c) x=0.4 and (d) x=0.6

The Rietveld refinement method [36] has been used for structural analysis, and using the ReX is a powder diffraction software [37]. On the orthorhombic Pbnm (N° 62) space group, it is possible to refine all of the peaks of $La_{1-x}Bi_xFeO_3$($x$ = 0.0, 0.2, 0.4, and 0.6) samples. The calculated lattice parameters, unit cell volume, refinement factors are summarized in Table 1, and the final Rietveld refinement plot is presented in Fig. 3.

**Table 1.** Crystallographic parameters of $La_{1-x}Bi_xFeO_3$ samples as obtained from Rietveld refinement

| Samples | x=0.0 | x=0.2 | x=0.4 | x=0.6 |
|---|---|---|---|---|
| Lattice parameters (Å): | | | | |
| a | 5.5561 | 5.5513 | 5.5577 | 5.5522 |
| b | 5.5679 | 5.5695 | 5.5788 | 5.5905 |
| c | 7.8428 | 7.8542 | 7.8438 | 7.8395 |
| Unit cell volume ($Å^3$): | | | | |
| V | 242.62 | 242.84 | 243.20 | 243.33 |
| Fit goodness: | | | | |
| $R_p$ (%) | 11.42 | 7.49 | 12.84 | 14.28 |
| $R_{wp}$ (%) | 17.39 | 12.81 | 17.96 | 20.40 |

The absence of a second phase in the doped samples shows that the $Bi^{3+}$ ions have completely dissolved into the host lattice by taking the place of the $La^{3+}$. The $La_{1-x}Bi_xFeO_3$ ($0 \le x \le 0.6$) unit cell volume is constant in the range of the error standard deviation (e.s.d.) with the addition of Bi. This result is due to the very closeradius of $Bi^{3+}$ion ($r(Bi^{3+})$= 1.17 Å) compared to the $La^{3+}$ ion ($r(La^{3+})$=1.16 Å) [38], which is evident from the XRD peak's slight shift towards a higher 2θ value in Fig. 3.

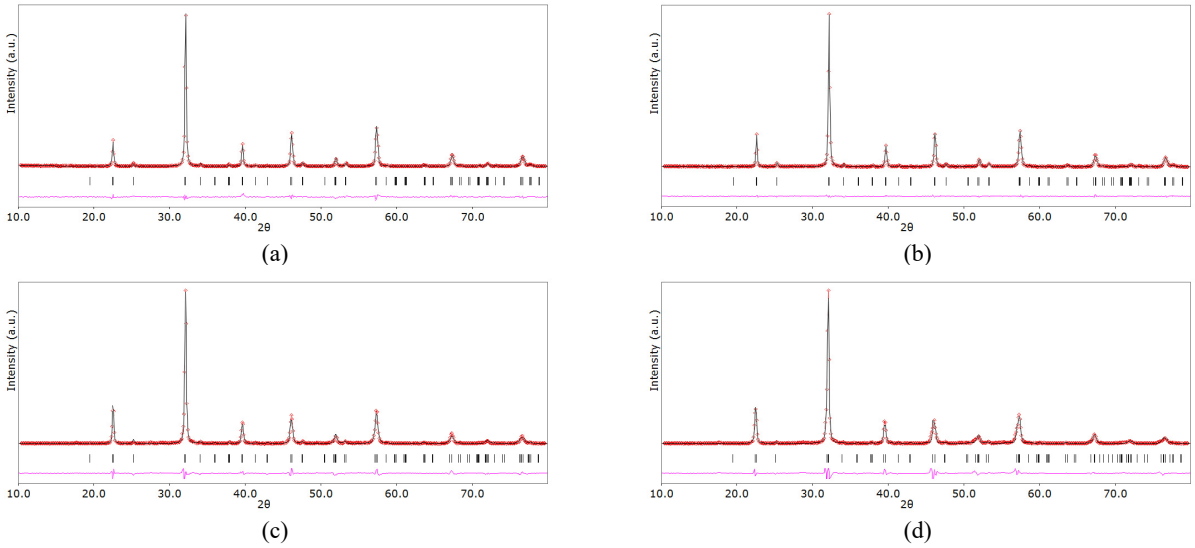


**Figure 3.** Rietveld refinement of experimental XRD pattern of $La_{1-x}Bi_xFeO_3$ samples (a) x=0.0, (b) x=0.2, (c) x=0.4 and (d) x=0.6 refined at room temperature

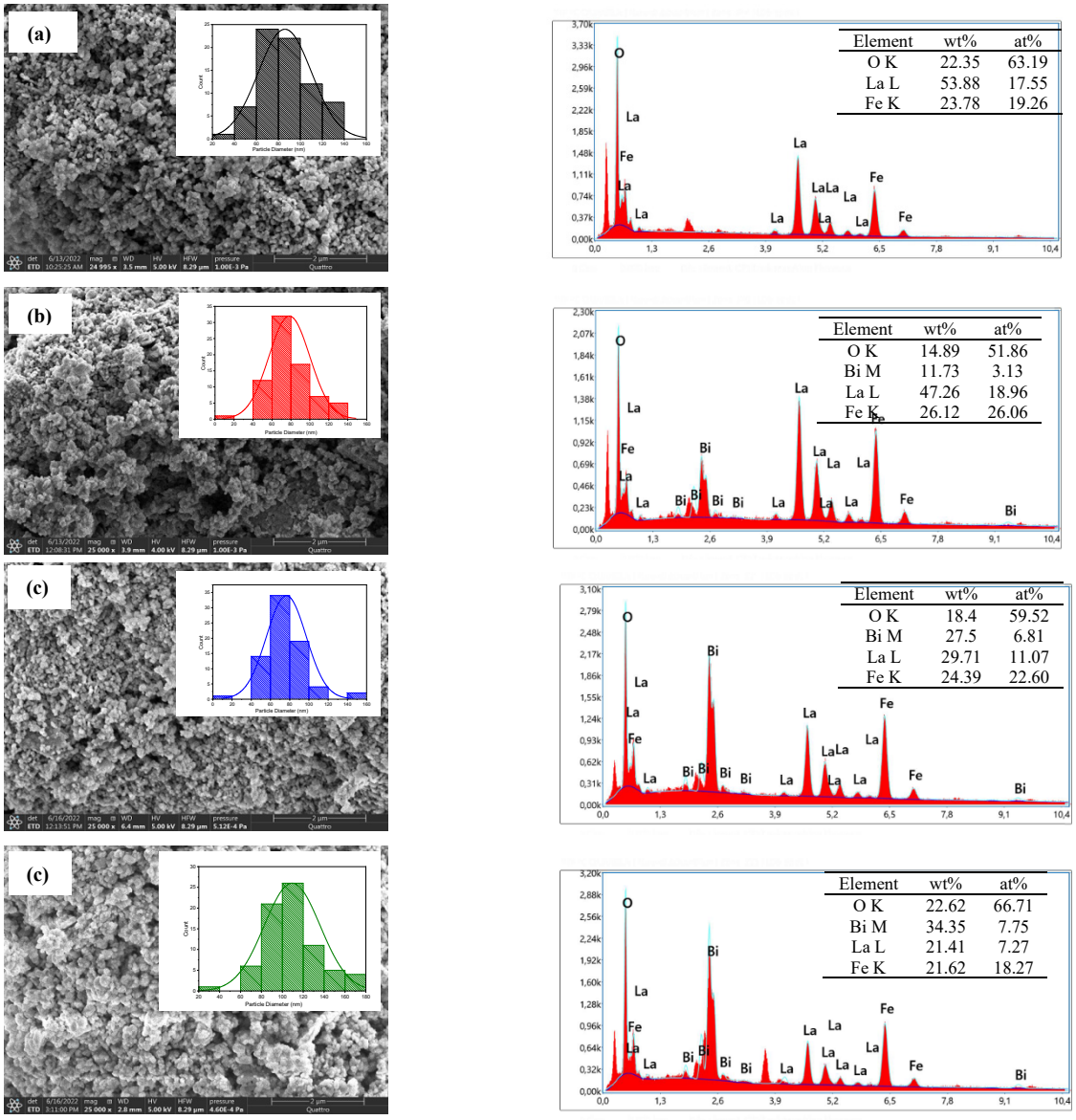


**Figure 4.** SEM morphology and EDX spectra of $La_{1-x}Bi_xFeO_3$ samples (a) x=0.0, (b) x=0.2, (c) x=0.4 and (d) x=0.6

Using spot measurements on powder samples, energy dispersive x-ray (EDX) spectroscopy was used to determine the quantitative composition of pure and $Bi^{3+}$-substituted $LaFeO_3$ nanoparticles. Within the limit of experimental error, the EDX analysis shows consistency with the predicted stoichiometry. The EDX spectrum confirms the desired samples (Fig. 4). Also, scanning electron microscopy (SEM) was utilized to examine the surface morphology of the prepared samples. As illustrated in Figure 4, the morphology of the studied samples shows a spherical shape of grains, similar to that of sand grains.

Both the dispersion and morphology of grains remained largely unchanged despite doping samples with $Bi^{3+}$ ions. However, as the concentration of Bi substitution increased, agglomerated spherical particles began to form and grew in size.

## FTIR Analysis

Figure 5 displays the FTIR spectra of pure and Bi-substituted $LaFeO_3$ in the range of [2000-450] $cm^{-1}$. It is important to note that the respective spectral ratios are almost similar from one to another, differing primarily in peak intensity. This difference can be attributed to variations in molar concentration composition. The strong absorption band at approximately 536 $cm^{-1}$ can be attributed to the (Fe-O) bending vibration characteristics of the octahedral $FeO_6$ groups in $La_{1-x}Bi_xFeO_3$. Additionally, the bands between 700 and 400 $cm^{-1}$ are mainly attributed to the formation of metal oxides [39].

On the other hand, the bending vibration of the La-O bonds may be responsible for the bands 717 $cm^{-1}$ [23]. Additionally, we observe that there are two closely bands, the first of which is at 1385 $cm^{-1}$and the second at 1485 $cm^{-1}$. They are attributed to $NO_3^-$ and N-H respectively, and both come from reacted precursor raw materials; they are neighbors and weak [40].

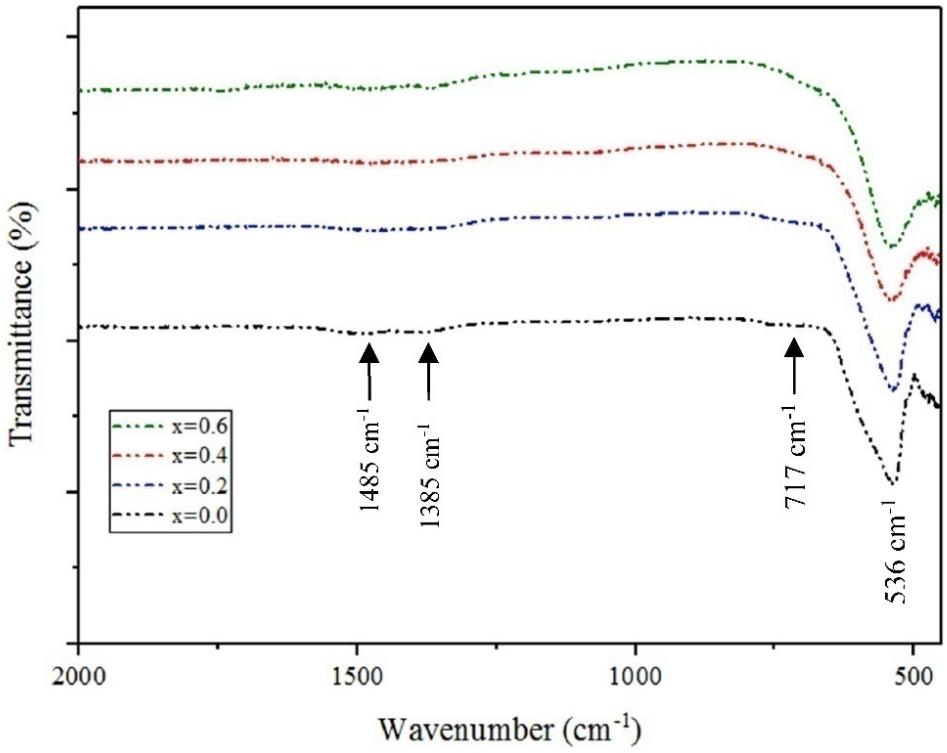


**Figure 5.** FTIR spectra of $La_{1-x}Bi_xFeO_3$ ($x$=0.0, 0.2, 0.4 and 0.6) nanoparticles

The La/Fe-O bending vibration modes do not change in frequency with increasing Bi content up to x=0.6, confirming that there has been no lattice deformation and, consequently, no changes in the length of the La/Fe-O bond, as supported by the XRD analysis.

## Optical Study

In order to describe the optical properties of the $La_{1-x}Bi_xFeO_3$ ($x$=0.0, 0.2, 0.4 and 0.6) nanoparticles, UV-Visible spectroscopy is used. From Tauc's plot, the bandgaps of the prepared samples were taken. Tauc's equation [41] mentioned below in eqt. 2 can be used to calculate the relationship between absorption coefficient ($\alpha$) and incident photon energy ($h\upsilon$).

$$(\alpha h\upsilon)^2 = A(h\upsilon - E_g) \quad (2)$$

where α is the optical absorption coefficient, hν is the photon energy, $E_g$ is the direct band gap, and A is constant.

$E_g$ for direct transitions is obtained by extrapolating the linear parts of the curves toward absorption equal to zero (Fig. 6). Pure $LaFeO_3$is thought to have a direct band gap of 2.2 eV. However, $E_g$ values decrease to 1.86, 1.76, and1.54 eV, respectively, for Bi substitutions of 20, 40, and 60%.

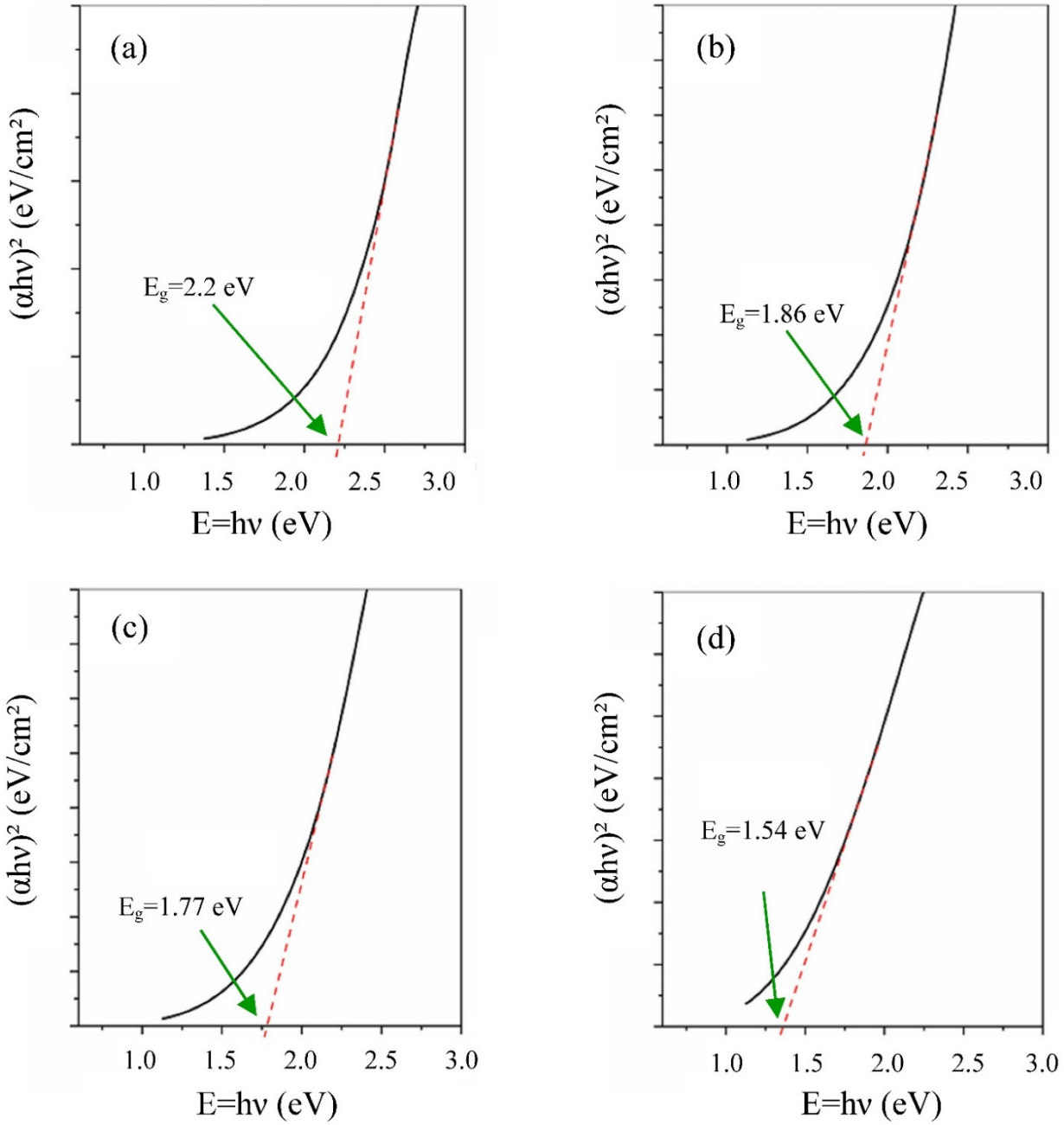


**Figure 6.** Tauc plots for optical absorption curves of $La_{1-x}Bi_xFeO_3$ samples (a) x=0.0, (b) x=0.2, (c) x=0.4, and (d) x=0.6.

Furthermore, the value of $E_g$ can be decreased through Fe–O octahedral restructuring of molecular orbitals and nanoparticles length scale [42–44]. This reduction could also be attributed to the direct energy transfer occurring between the excited states of the semiconductor and the 3d levels of $Bi^{3+}$ ions [45].

**Evaluation of the Photocatalytic Efficiency**

The photocatalytic degradation of O-toluidine blue (o-TB) was examined using $La_{1-x}Bi_xFeO_3$ ($x$ = 0.0, 0.2, 0.4, 0.6) under the influence of solar irradiation. The results show that most of the o-TB dye is removed within 60 minutes (Fig. 7).

Table 2 shows that the photocatalytic activity of $La_{1-x}Bi_xFeO_3$ (x = 0.0, 0.2, 0.4 and 0.6) samples decreases with an increase in their average grain size. This can be attributed to the fact that smaller particle size with a larger surface area per unit volume provide more active sites for photocatalytic reactions, leading to a higher photocatalytic degradation rate, especially in the case of spherical nanoparticles with smaller particle sizes [46-48]. This principle applies to the spherical shape of the grain morphology in the studied samples.

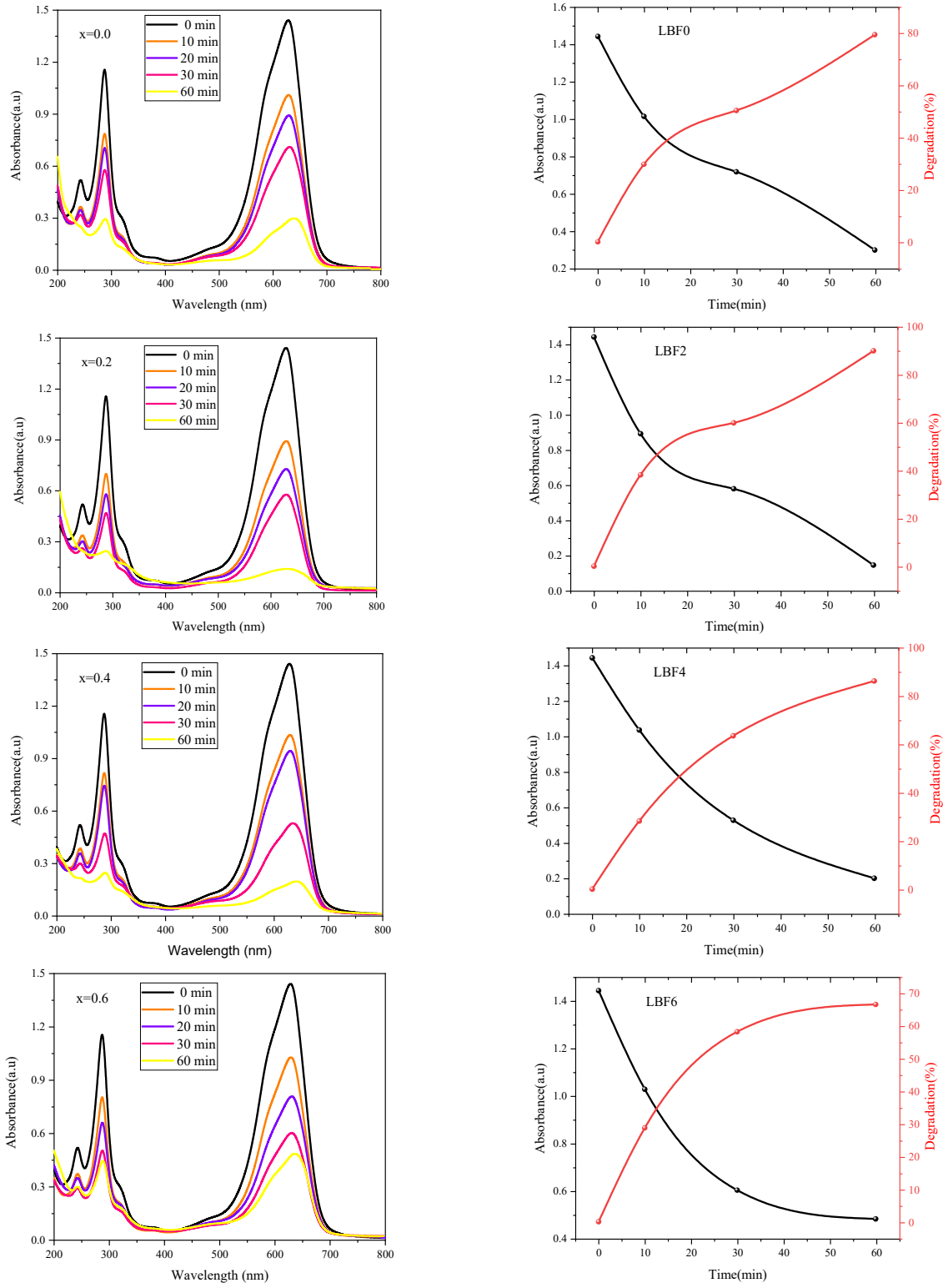


**Figure 7.** UV-Vis time-dependent absorption spectrum during the photocatalytic reaction of o-TB for $La_{1-x}Bi_xFeO_3$ (x = 0.0, 0.2, 0.4 and 0.6) samples

**Table 2.** Photocatalytic activity vs. Average particle size for $La_{1-x}Bi_xFeO_3$ (x = 0.0, 0.2, 0.4 and 0.6) samples.

| Catalyst | Photocatalytic activity (%) | Average particle size (nm) |
|---|---|---|
| $LaFeO_3$ | 79.50 | 85 |
| $La_{0.8}Bi_{0.2}FeO_3$ | 90.09 | 76 |
| $La_{0.6}Bi_{0.4}FeO_3$ | 86.28 | 78 |
| $La_{0.4}Bi_{0.6}FeO_3$ | 66.68 | 108 |

The highest photocatalytic activity (90.09%) was observed for $La_{0.8}Bi_{0.2}FeO_3$, which has the smallest average grain size (76 nm). Additionally, the photocatalytic activity of $La_{0.6}Bi_{0.4}FeO_3$ (78 nm) was slightly lower (86.28%), but still higher than that of $LaFeO_3$ (79.50%) and $La_{0.4}Bi_{0.6}FeO_3$, which exhibited a rate of 66.68% (Fig. 7). Therefore, these results support the notion that the average grain size and the shape of grains are an important factor in determining the photocatalytic activity of $La_{1-x}Bi_xFeO_3$.

In contrast, data obtained by Mocwana et al. [32] indicate that the optimal degradation rates for o-TB, using $LaFeO_3$ nanosheets, resulted in a catalytic degradation of 37% over 30 minutes. Notably, this rate remains lower than all the values obtained in our experiments for the same duration.

Furthermore, it was observed that an increase in the amount of Bi up to 20% within 60 minutes of the reaction time significantly enhances removal efficiency. This improvement can be attributed to the increased formation of hydroxyl radicals.

Conversely, a further increase in the Bi ratio decreases the removal efficiency of the o-TB dye. This can be attributed to (i) the increase in the average grain sizes, and (ii) the blocking of UV light penetration with an increasing amount of Bi [49, 50].

This can be interpreted as when the catalyst load is small, the catalyst absorbs fewer photons for the photocatalytic reaction, resulting in lower photocatalytic activity. As the catalyst loading increases, the number of photon absorption centers and activity centers on the catalyst surface increases, thereby increasing the catalyst's activity. However, with further increases in catalyst loading, the number of photons tends to become saturated. This heightened catalyst loading may lead to light blockage, consequently affecting the photocatalytic efficiency [51]. Thus, the narrow band gap value of $La_{0.8}Bi_{0.2}FeO_3$ (1.86 eV) nanoparticle suggests its potential as a promising candidate for the excellent purification of wastewater containing o-TB dye.

## CONCLUSIONS

In conclusion, the perovskite-type $La_{1-x}Bi_xFeO_3$ photocatalysts was successfully synthesized using the modified Pechini route, and their performance for photodegradation of o-TB dye wastewater was studied. XRD and EDX combination studies proved that all samples have an orthorhombic structure with a single-crystalline orthorhombic structure, and the average grain size samples increased by increasing of Bi-substitution to be 85 nm, 76 nm, 78 nm, and 108 nm for x=0.0, 0.2, 0.4, and 0.6 respectively. Morphological and optical properties of the perovskite-type $La_{1-x}Bi_xFeO_3$samples exhibited a well-crystalline form and excellent band gap energy respectively. A photocatalytic reaction was conducted to test the degradation ability of the synthesized samples towards o-TB dye. The reaction was monitored over a period of 60 min while using the UV-Vis to observe the degradation activity. The most photocatalytically active sample for decomposition of o-TB under visible light was $La_{0.8}Bi_{0.2}FeO_3$. This nanoparticle acts as an excellent photocatalyst for the degradation of o-TB dye with 90.09% efficiency in 60 min under natural sunlight irradiation. This sample have the smallest average grain size and a band gap energy in the range of semiconductor materials. These results give hope for future application of this material in photocatalytic degradation of various organic pollutants present in polluted water under natural sunlight. Hence, this nanoparticle may be well exploited for the remediation of the polluted water under natural sunlight on a large scale.

**Acknowledgements**

The authors gratefully acknowledge the financial support of Directorate General for Scientific Research and Technological Development –DGRSDT– (PRFU Project N°. B00L02UN390120180003), Ministry of Higher Education and Scientific Research – ALGERIA.

## ORCID

**Mohammed Sadok Mahboub,** https://orcid.org/0000-0001-5495-5249; **Soria Zeroual**, https://orcid.org/0000-0002-5922-9980
**Samir Bayou,** https://orcid.org/0000-0001-8553-3428; **Mebrouk Ghougali,** https://orcid.org/0000-0003-0496-4555
**Adel Benarfa**, https://orcid.org/0000-0002-0377-0161; **Souhaila Meneceur,** https://orcid.org/0000-0002-6890-3762

## REFERENCES

[1] M. Strokal, Z. Bai, W. Franssen, et al., "Urbanization: an increasing source of multiple pollutants to rivers in the 21st century," NPJ Urban Sustain, **1**, 24 (2021). https://doi.org/10.1038/s42949-021-00026-w
[2] Z.N. Garba, W. Zhou, M. Zhang, and Z. Yuan, "A review on the preparation, characterization and potential application of perovskites as adsorbents for wastewater treatment," Chemosphere, **244**, 125474 (2020). https://doi.org/10.1016/j.chemosphere.2019.125474
[3] L. Lin, H. Yang, and X. Xu, "Effects of Water Pollution on Human Health and Disease Heterogeneity: A Review," Front. Environ. Sci. **10**, 880246 (2022). https://doi.org/10.3389/fenvs.2022.880246
[4] A. Zhitkovich, "Chromium in Drinking Water: Sources, Metabolism, and Cancer Risks," Chem. Res. Toxicol., **24**(10), 1617–1629 (2011). https://doi.org/10.1021/tx200251t
[5] S.K. Gupta, R.C. Gupta, A.B. Gupta, A.K. Seth, J.K. Bassin, and A. Gupta, "Recurrent acute respiratory tract infections in areas with high nitrate concentrations in drinking water," Environmental health perspectives, **108**(4), 363–366 (2000). https://doi.org/10.1289/ehp.00108363
[6] C.L. Gray, D.T. Lobdell, K.M. Rappazzo, Y. Jian, J.S. Jagai, L.C. Messer, A.P. Patel, et al., "Associations between environmental quality and adult asthma prevalence in medical claims data," Environ Res., **166**, 529–536 (2018). https://doi.org/10.1016/j.envres.2018.06.020

[7] S.T. Matsumoto, M.S. Mantovani, M.I.A. Malaguttii, A.L. Dias, I.C. Fonseca, and M.A. Marin-Morales, "Genotoxicity and mutagenicity of water contaminated with tannery effluents, as evaluated by the micronucleus test and comet assay using the fish Oreochromis niloticus and chromosome aberrations in onion root-tips," Genetics and Molecular Biology, **29**(1), 148–158 (2006). https://doi.org/10.1590/S1415-47572006000100028
[8] J.H. Wang, J. Qiao, J.L. Tu, and X.-H. Huang, "Research Progress on Photocatalytic Degradation of Dye by Perovskite-type Metal Oxides (In Chinese)," Rare Metals and Cemented Carbides, **41**(1), 50–54 (2013).
[9] J.A. Silva, "Wastewater Treatment and Reuse for Sustainable Water Resources Management: A Systematic Literature Review," Sustainability, **15**(14), 10940 (2023). https://doi.org/10.3390/su151410940
[10] S.K. Loeb, P.J.J. Alvarez, J.A. Brame, E.L. Cates, W. Choi, J. Crittenden, D.D. Dionysiou, et al., "The Technology Horizon for Photocatalytic Water Treatment: Sunrise or Sunset?" Environ. Sci. Technol., **53**(6), 2937–2947 (2019). https://doi.org/10.1021/acs.est.8b05041
[11] M.N. Chong, B. Jin, C.W.K. Chow, and C. Saint, "Recent developments in photocatalytic water treatment technology: A review," Water Research, **44**(10), 2997–3027 (2010). https://doi.org/10.1016/j.watres.2010.02.039
[12] J.Blanco-Galvez, P.Fernández-Ibáñez, and S. Malato-Rodríguez, "Solar photocatalytic detoxification and disinfection of water: recent overview," J. Sol. Energy Eng., **129**(1), 4–15 (2007). https://doi.org/10.1115/1.2390948
[13] S.D. Khairnar, and V.S. Shrivastava, "Facile Synthesis of Nickel Oxide Nanoparticles for the Degradation of Methylene Blue and Rhodamine B dye: A Comparative Study," J. Taibah. Univ. Sci., **13**, 1108–1118 (2019). https://doi.org/10.1080/16583655.2019.1686248
[14] V.A. Adole, T.B. Pawar, P.B. Koli, and B.S. Jagdale, "Exploration of Catalytic Performance of Nano-$La_2O_3$ as an Efficient Catalyst for Dihydropyrimidinone/Thione Synthesis and gas Sensing," J. Nanostructure Chem., **9**, 61–76 (2019). https://doi.org/10.1007/s40097-019-0298-5
[15] A. Fujishima, and K. Honda, "Electrochemical photolysis of water at a semiconductor electrode," Nature, **238**(5358), 37–38 (1972). https://doi.org/10.1038/238037a0
[16] S. Singh, H. Mahalingam, and P.K. Singh, "Polymer-supported Titanium Dioxide Photocatalysts for Environmental Remediation: A Review," Appl. Catal. A: Gen., **462-463**, 178–195 (2013). https://doi.org/10.1016/j.apcata.2013.04.039
[17] R.S. Shinde, S.D. Khairnar, M.R. Patil, V.A. Adole, P.B. Koli, V.V. Deshmane, D.K. Halwar, et al., "Synthesis and Characterization of ZnO/CuO Nanocomposites as an Effective Photocatalyst and gas Sensor for Environmental Remediation," J. Inorg. Organomet. Polym., **32**, 1045–1066, (2022). https://doi.org/10.1007/s10904-021-02178-9
[18] M. Periyasamy, and A. Kar, "Modulating the Properties of $SnO_2$ Nanocrystals: Morphological Effects on Structural, Photoluminescence, Photocatalytic, Electrochemical and gas Sensing Properties," J. Mater. Chem. C,**8**, 4604–4635 (2020). https://doi.org/10.1039/C9TC06469A
[19] C. Xu, P.R. Anusuyadevi, C. Aymonier, R. Luque, and S. Marre, "Nanostructured Materials for Photocatalysis," Chem. Soc. Rev., **48**, 3868–3902 (2019). https://doi.org/10.1039/C9CS00102F
[20] S. Dhariwal, and M. Mittal, "Wastewater treatment with perovskite-based photocatalysts: Environmental sustainability from a green perspective," Materials Today: Proceedings, (2023). https://doi.org/10.1016/j.matpr.2023.03.048
[21] N.N. Toan, S. Saukko, and V. Lantto, "Gas sensing with semiconducting perovskite oxide $LaFeO_3$,"Physica B: Condensed Matter, **327**(2–4), 279–282 (2003). https://doi.org/10.1016/S0921-4526(02)01764-7
[22] N.S. Tijare, V.M. Joshi, S.P. Padole, A.P. Manguklar, S.S. Rayalu, and K.N. Labhsetwar, "Photocatalytic hydrogen generation through water splitting on nano-crystalline $LaFeO_3$ perovskite," Int. J. Hydrog. Energy, **37**, 10451–10456 (2012). https://doi.org/10.1016/j.ijhydene.2012.01.120
[23] M. Ismael, and M. Wark, "Perovskite-type $LaFeO_3$: Photoelectrochemical Properties and Photocatalytic Degradation of Organic Pollutants Under Visible Light Irradiation," Catalysts, **9**(4), 342 (2019). https://doi.org/10.3390/catal9040342
[24] L. Li, L. Pan, D. Zhang, and J. Rong, "Ultrasonic-assisted synthesis of $LaFeO_3$/$CeO_2$ heterojunction for enhancing the photocatalytic degradation of organic pollutants," Materials Science in Semiconductor Processing, **152**, 107058 (2022). https://doi.org/10.1016/j.mssp.2022.107058
[25] X.J. Wang, H.Y. Shen, H.Y. Tian, and Q.H. Yang, "Photocatalytic Degradation of Water-Soluble Azo Dyes by $LaFeO_3$ and $YFeO_3$," Adv. Mater. Res., **465**, 37–43 (2012). https://doi.org/10.4028/www.scientific.net/AMR.465.37
[26] L. Hou, G. Sun, K. Liu, Y. Li, and F. Gao, "Preparation, characterization and investigation of catalytic activity of Li-doped $LaFeO_3$ nanoparticles," J. Sol-Gel Sci. Technol., **40**, 9–14 (2006). https://doi.org/10.1007/s10971-006-8368-9
[27] P. Tang, M. Fu, H. Chen, and F. Cao, "Synthesis of Nanocrystalline $LaFeO_3$ by Precipitation and its Visible-Light Photocatalytic Activity," Mater. Sci. Forum, **694**, 150–154 (2011). https://doi.org/10.4028/www.scientific.net/MSF.694.150
[28] S. Thirumalairajan, K. Girija, R.V. Masteralo, and N. Ponpandian, "Photocatalytic degradation of organic dyes under visible light irradiation by floral-like $LaFeO_3$ nanostructures comprised of nanosheet petals," New J. Chem., **38**, 5480–5490 (2014). https://doi.org/10.1039/C4NJ01029A
[29] H. Wu, R. Hu, T. Zhou, C. Li, W. Meng, and J. Yang, "A Novel Efficient Boron-Doped $LaFeO_3$ Photocatalyst with Large Specific Surface Area for Phenol Degradation Under Simulated Sunlight," CrystEngComm, **17**, 3859–3865 (2015). https://doi.org/10.1039/C5CE00288E
[30] S. Thirumalairajan, K. Girija, I. Ganesh, D. Mangalaraj, C. Viswanathan, A. Balamurugan, and N. Ponpandian, "Controlled synthesis of perovskite $LaFeO_3$ microsphere composed of nanoparticles via self-assembly process and their associated photocatalytic activity," Chem. Eng. J., **209**, 420–428 (2012). https://doi.org/10.1016/j.cej.2012.08.012
[31] H. Deng, Z. Mao, H. Xu, L. Zhang, Y. Zhong, and X. Sui, "Synthesis of fibrous $LaFeO_3$ perovskite oxide for adsorption of Rhodamine B," Ecotoxicol. Environ. Saf., **168**, 35–44 (2019). https://doi.org/10.1016/j.ecoenv.2018.09.056
[32] M.L. Mocwana, P.P. Mokoena, P.S. Mbule, I.N. Beas, G.L. Kabongo, S.N. Ogugua, and T.E. Tshabalala, "Photocatalytic Degradation of Methylene Blue and Ortho-Toluidine Blue: Activity of Lanthanum Composites $La_xMO_y$ (M: Fe, Co, Ni)," Catalysts., **12**(11),1313 (2022). https://doi.org/10.3390/catal12111313
[33] M. Dhiman, and S. Singhal, "Effect of Doping of Different Rare Earth (Europium, Gadolinium, Dysprosium and Neodymium) Metal Ions on Structural, Optical and Photocatalytic Properties of $LaFeO_3$ Perovskites," J. Rare. Earth, **37**, 1279–1287 (2019). https://doi.org/10.1016/j.jre.2018.12.015

[34] T.T.N. Phan, A.N. Nikoloski, P.A. Bahri, and D. Li, "Heterogeneous Photo-Fenton Degradation of Organics Using Highly Efficient Cu-Doped $LaFeO_3$ Under Visible Light," J. Indus. Eng. Chem, **61**, 53–64 (2018). https://doi.org/10.1016/j.jiec.2017.11.046
[35] X.-T. Yin, H. Huang, J.-L. Xie, D. Dastan, J. Li, Y. Liu, X.-M. Tan, X.-C. Gao, W. A. Shah, and X.-G. Ma, "High-performance visible-light active Sr-doped porous $LaFeO_3$ semiconductor prepared via sol–gel method," Green Chemistry Letters and Reviews, **15**(3), 546–556 (2022). https://doi.org/10.1080/17518253.2022.2112093
[36] G. Will, "Powder Diffraction: The Rietveld Method and the Two Stage Method to Determine and Refine Crystal Structures from Powder Diffraction Data," Berlin Heidelberg: Springer-Verlag, 2006.
[37] M. Bortolotti, L. Lutterotti, and I. Lonardelli, "ReX: a computer program for structural analysis using powder diffraction data," J. Appl. Cryst., **42**, 538–539 (2009). https://doi.org/10.1107/S0021889809008309
[38] R.D. Shannon, "Revised effective ionic radii and systematic studies of interatomic distances in halides and chalcogenides," Acta Crystallogr. A, **32**, 751–767 (1976). https://doi.org/10.1107/s0567739476001551
[39] M. Čebela, B. Janković, R. Hercigonja, M.J. Lukić, Z. Dohčević-Mitrović, D. Milivojević, and B. Matović, "Comprehensive characterization of $BiFeO_3$ powder synthesized by the hydrothermal procedure," Processing and Application of Ceramics, **10**(4), 201–208 (2016). https://doi.org/10.2298/PAC1604201C
[40] P. Desai, and A. Athawale, "Microwave Combustion Synthesis of Silver Doped Lanthanum Ferrite Magnetic Nanoparticles," Defence Science Journal, **63**(3), 285–291 (2013). https://doi.org/10.14429/dsj.63.2387
[41] J.I. Pankove, "Optical Processes in Semiconductors", New Jersey: Prentice-Hall, Englewood Cliffs, 1971.
[42] M. Sivakumar, A. Gedanken, W. Zhong, Y.H. Jiang, Y.W. Du, I. Brukental, D. Bhattacharya, Y. Yeshurun, and I. Nowik, "Sonochemical synthesis of nanocrystalline $LaFeO_3$," J. Mater. Chem., **14**, 764–769 (2004). https://doi.org/10.1039/B310110J
[43] M. Popa, J. Frantti, and M. Kakihana, "Lanthanum ferrite $LaFeO_{3+d}$ nanopowders obtained by the polymerizable complex method," Solid State Ionics, **154**, 437–445 (2002). https://doi.org/10.1016/S0167-2738(02)00480-0
[44] M.A. Matin, M.N. Hossain, M.M. Rhaman, F.A. Mozahid, M.A. Ali, M.A. Hakim, and M.F. Islam, "Dielectric and optical properties of Ni-doped $LaFeO_3$ nanoparticles," SN Appl. Sci., **1**, 14792 (2019). https://doi.org/10.1007/s42452-019-1453-9
[45] F. J. Brieler, M. Fröba, L. Chen, P. J. Klar, W. Heimbrodt, H.A.K. von Nidda, and A. Loidl, "Ordered Arrays of II/VI Diluted Magnetic Semiconductor Quantum Wires: Formation within Mesoporous MCM-41 Silica," Chem. Eur. J., **8**(1), 185–194 (2002). https://doi.org/10.1002/1521-3765(20020104)8:1<185::AID-CHEM185>3.0.CO;2-L
[46] C. Retamoso, N. Escalona, M. González, L. Barrientos, P. Allende-González, S. Stancovich, R. Serpell, J. L. G. Fierro, and M. Lopez, "Effect of particle size on the photocatalytic activity of modified rutile sand ($TiO_2$) for the discoloration of methylene blue in water," Journal of Photochemistry and Photobiology A: Chemistry, **378**, 136–141 (2019). https://doi.org/10.1016/j.jphotochem.2019.04.021
[47] Z. Cui, L. Zhang, Y. Xue, Y. Feng, M. Wang, J. Chen, B. Ji, C. Wang, and Y. Xue, "Effects of shape and particle size on the photocatalytic kinetics and mechanism of nano-$CeO_2$," Int. J. Miner. Metall. Mater., **29**(12), 2221–2231 (2022). https://doi.org/10.1007/s12613-021-2332-0
[48] S. Chaturvedi, P.N. Dave, and N.K. Shah, "Applications of nano-catalyst in new era," Journal of Saudi Chemical Society, **16**(3), 307–325 (2012). https://doi.org/10.1016/j.jscs.2011.01.015
[49] M. Saquib, M. Abu Tariq, M. M. Haque, and M. Muneer, "Photocatalytic degradation of disperse blue 1 using UV/$TiO_2$/$H_2O_2$ process," Journal of Environmental Management, **88**(2), 300–306 (2008). https://doi.org/10.1016/j.jenvman.2007.03.012
[50] H. A. M. Salim, and S. A. M. Salih, "Photodegradation Study of Toluidine Blue Dye in Aqueous Solution using Magnesium Oxide as a Photocatalyst," Int. Journal of Chemistry, **7**(2), 143–149 (2015). https://doi.org/10.5539/ijc.v7n2p143
[51] D. Zhang, S. Lv, and Z. Luo, "A study on the photocatalytic degradation performance of a $[KNbO_3]_{0.9}$-$[BaNi_{0.5}Nb_{0.5}O_{3-d}]_{0.1}$ perovskite," RSC Adv., **10**, 1275–1280 (2020). https://doi.org/10.1039/c9ra07310h

## $La_{0.8}Bi_{0.2}FeO_3$ ПЕРОВСКІТНОГО ТИПУ: ВИСОКА ЕФЕКТИВНІСТЬ ФОТОКАТАЛІТИЧНОЇ ДЕГРАДАЦІЇ ОРТОТОЛУЇДИНОВОГО СИНЬОГО ПІД ОПРОМІНЕННЯМ ВИДИМИМ СВІТЛОМ

**Уарда Бен Алі[a], Мохаммед Садок Махбуб[a], Сорія Зеруал[a], Самір Баю[b], Азеддін Беггас[a], Мебрук Гугалім, Адель Бенарфа[c], Сухайла Менесер[d]**

[a] *Лабораторія LEVRES, Університет Ель-Уед, 39000 Ель-Уед, Алжир*
[b] *Хімічний факультет, факультет точних наук, Університет Ель-Уед, 39000 Ель-Уед, Алжир*
[c] *Центр наукових і технічних досліджень фізико-хімічного аналізу (CRAPC)-PTAPC, P.O. Box 0354, Лагуат 03000, Алжир*
[d] *Лабораторія біотехнології біоматеріалу та конденсованих речовин, Технологічний факультет, Університет Ель-Уеда, Ель-Уед 39000, Алжир*

У цьому дослідженні наночастинки перовскіту $La_{1-x}Bi_xFeO_3$ (x=0,0, 0,2, 0,4 і 0,6) були синтезовані модифікованим методом Пекіні. Ретельний аналіз за допомогою XRD та SEM/EDX підтвердив відсутність вторинних фаз як у чистих, так і в Bi-заміщених зразках $LaFeO_3$, що вказує на утворення однофазного перовскіту. СЕМ-зображення виявили квазісферичну форму частинок. Фотокаталітичну активність $La_{1-x}Bi_xFeO_3$ (x=0,0, 0,2, 0,4 і 0,6) оцінювали за деградацією орто-толуїдинового синього під опроміненням видимим світлом, що вказує на те, що $La_{0.8}Bi_{0.2}FeO_3$ демонструє чудову фотокаталітичну активність. Загальна швидкість видалення o-Toluidine Blue досягла 90,09% після опромінення видимим світлом протягом 60 хв. Ми пояснюємо цю підвищену фотокаталітичну активність розміром зерна та оптичними властивостями підготовленого зразка. Отже, $La_{0.8}Bi_{0.2}FeO_3$ можна розглядати як дуже перспективний фотокаталізатор у майбутньому промисловому застосуванні для ефективного очищення стічних вод від барвників.

**Ключові слова:** *$La_{1-x}Bi_xFeO_3$; барвник орто-толуїдиновий синій; модифікований метод Печіні; фотокаталіз видимим світлом; очищення стічних вод*